A numerical study of the effects of superhydrophobic surface on skin-friction drag in turbulent channel flow

Hyunwook Park, Hyungmin Park, and John Kim

A numerical study of the effects of superhydrophobic surface on skin-friction drag in turbulent channel flow

Hyunwook Park, Hyungmin Park,[a] and John Kim[b]
*Mechanical and Aerospace Engineering Department, University of California,
Los Angeles, California 90095, USA*

Superhydrophobic surfaces have attracted much attention lately as they present the possibility of achieving a substantial skin-friction drag reduction in turbulent flows. In this paper, the effects of a superhydrophobic surface, consisting of microgrates aligned in the flow direction, on skin-friction drag in turbulent flows were investigated through direct numerical simulation of turbulent channel flows. The superhydrophobic surface was modeled through a shear-free boundary condition on the air-water interface. Dependence of the effective slip length and resulting skin-friction drag on Reynolds number and surface geometry was examined. In laminar flows, the effective slip length depended on surface geometry only, independent of Reynolds number, consistent with an existing analysis. In turbulent flows, the effective slip length was a function of Reynolds number, indicating its dependence on flow conditions near the surface. The resulting drag reduction was much larger in turbulent flows than in laminar flows, and near-wall turbulence structures were significantly modified, suggesting that indirect effects resulting from modified turbulence structures played a more significant role in reducing drag in turbulent flows than the direct effect of the slip, which led to a modest drag reduction in laminar flows. It was found that the drag reduction in turbulent flows was well correlated with the effective slip length normalized by viscous wall units. © *2013 AIP Publishing LLC.* [http://dx.doi.org/10.1063/1.4819144]

I. INTRODUCTION

Superhydrophobic surfaces (SHSs), a combination of hydrophobicity and surface roughness in micro- and/or nano-scales, lower the free energy of an air-water interface such that a water droplet on the surface has a very high contact angle ($\geq 150°$). In certain situations, air pockets are stably entrapped between the surface features [Fig. 1(a)], thereby creating a significant effective slip length (λ) on the surface [Fig. 1(b)], fully submerged in moving water.[1,2] SHSs with an effective slip length on the order of 200–400 μm have been reported.[3,4] Different applications of SHSs (e.g., skin-friction drag reduction,[2] self-cleaning,[5] microfluidic devices,[6] anti-biofouling,[7] and anti-fogging/icing,[8] to name a few) have been explored. One of the highly anticipated benefits of SHSs is reduction of skin-friction drag on solid objects moving in water, thereby achieving significant energy savings and reduction of greenhouse gas emissions. The prospect of reducing skin-friction drag without additional energy input, in contrast to other active control schemes (e.g., injection of air bubbles, surface blowing, and suction), has been the primary reason for interest in SHSs.

Some key aspects of SHSs relevant to skin-friction drag reduction have been investigated: e.g., how to increase the effective slip length,[3,4] how to improve the stability of underwater superhydrophobic states,[9] and how to maintain those superhydrophobic states under water while overcoming adverse conditions.[10] Despite these efforts, experimental observations of noticeable drag reduction

---

[a]Present address: Department of Mechanical & Aerospace Engineering, Seoul National University, Seoul 151-744, South Korea.
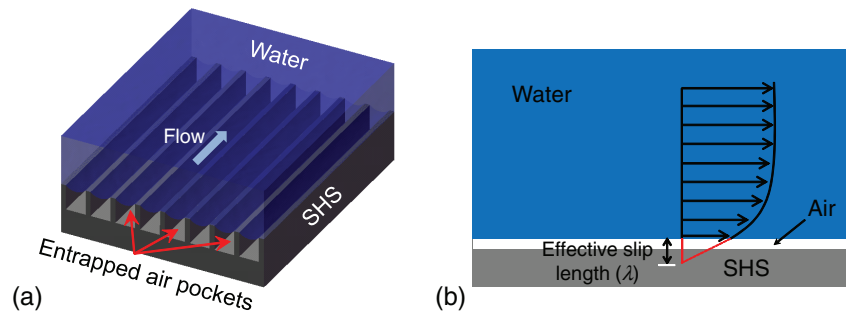[b]Author to whom correspondence should be addressed. Electronic mail: jkim@seas.ucla.edu

FIG. 1. (a) A schematic of water flow over an SHS with micrograftes aligned along the flow direction. (b) Definition of the effective slip length (λ).

on SHSs have been elusive and largely limited to laminar flows.[2] On the other hand, in numerical studies, where superhydrophobicity was assumed to prevail and SHSs were modeled through a boundary condition, several investigators have reported significant drag reduction in both laminar and turbulent channel flows. The drag reduction in laminar flows is a direct consequence of the effective slip on SHSs,[11,12] whereas the mechanism by which drag reduction was achieved in turbulent flows is not well understood. The objective of this numerical study is to gain further insight into the effects of superhydrophobic surface on skin-friction drag in turbulent flows.

This paper is organized as follows. A brief review of previous studies on the effects of SHSs on skin-friction drag is given in Sec. II. Details of numerical simulations are described in Sec. III. In Sec. IV, we discuss the present results, followed by a summary and concluding remarks in Sec. V.

In this paper, the superscript $^+$ denotes flow variables normalized by the wall-shear velocity, u_τ, and the kinematic viscosity, ν. Re_c (Re_τ) denotes Reynolds number based on the centerline velocity (wall-shear velocity) and the channel half width, δ.

II. PREVIOUS STUDIES

There have been several reviews of SHS research from various disciplines.[2,13–15] Some have evaluated natural and biomimetic characteristics of SHSs based on the liquid droplet dynamics in air (i.e., in terms of the apparent contact angle) and suggested their possible applications.[13] However, the droplet dynamics alone cannot explain how a relatively small slip length in micro scales on the order of micro meters can affect flow phenomena in macro scales (e.g., wall-shear stress).[14,15] Here we focus only on the fluid dynamic aspects of SHSs, especially regarding skin-friction drag in laminar and turbulent flows.

Skin-friction drag reduction on SHSs in laminar flows is relatively well understood through theoretical,[16] numerical,[11,17,18] and experimental studies.[1,11,12,19–22] In laminar flows, the effective slip, which is a manifestation of the modified mean velocity profile near the surface, directly affects the skin-friction drag.[11,12] Thus, for a given flow geometry, the theoretical prediction of drag reduction depends on the effective slip length only, independent of flow conditions such as Reynolds number. Figure 2 shows skin-friction drag in channel flows, normalized by the drag on a regular surface, as a function of the effective slip length normalized by the channel half width. The scatters are most likely due to experimental errors, illustrating that an accurate measurement of drag is difficult and important in assessing the performance of SHSs.

Numerical simulations have provided additional information about the effects of SHSs on laminar flows. Researchers at Brigham Young University[11,17,18] have simulated the flow in a microchannel with a superhydrophobic wall consisting of micrograftes aligned parallel (longitudinal) or normal (transverse) to the flow direction. Both longitudinal (i.e., with streamwise slip) and transverse (i.e., with spanwise slip) micrograftes were shown to reduce the skin-friction drag, while there is more drag reduction with the longitudinal grates.

So far, detailed investigations of the effects of SHSs on turbulent flows have been mostly performed by numerical studies of fully developed turbulent channel flows.[23–28] Air-water
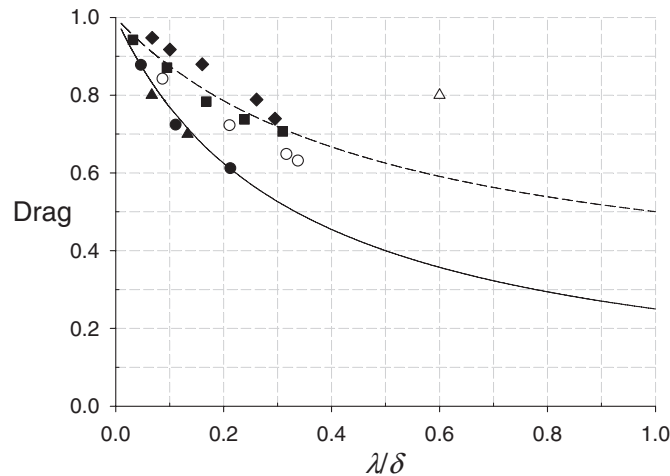
FIG. 2. Drag (normalized by the drag of regular surface) as a function of the effective slip length normalized by the channel half-width, δ: —, theory for SHSs on both channel walls;[1] – – –, theory for SHS on one channel wall;[20] ●, present study (simulation); ▲, Choi and Kim;[1] ■, Maynes *et al.*;[11] ◆, Jung and Bhushan;[22] ○, Ou *et al.*;[20] △, Truesdell *et al.*[21] (experiments except the simulated slip length in Maynes *et al.*[11]). Here, the closed and open symbols are for SHS(s) on both and one channel wall(s), respectively.

interfaces on SHSs were modeled either by a specified slip length[23, 24, 26] or by shear-free boundary condition.[25, 27, 28] In addition, the air-water interface was assumed to be a flat surface. In spite of these simplifications, many useful insights have been gained. With the same SHS, the drag reduction was found to be significantly larger in turbulent flows,[28] implying additional effects of SHSs than just the direct effect of the effective slip, which led drag reduction in laminar flows. It was also found that effective slip length must be on the order of the viscous sublayer thickness in order to have an impact on skin-friction drag in turbulent flows.[23] Busse and Sandham[24] found that the variation of turbulent skin-friction drag on a SHS was closely related to the changes in streamwise velocity and wall shear-stress fluctuations.

Despite many positive prospects revealed in numerical simulations, experimental confirmation of drag reduction on SHSs has been elusive. While some studies[22, 29–31] reported a noticeable amount (>10%) of drag reduction, others[32, 33] reported that their SHSs had a negligible effect on drag reduction in turbulent flows. This inconsistency, among other things, would be errors in measuring skin-friction drag, and partial or complete loss of air pockets in the presence of turbulence fluctuations. Recently, overcoming some of the earlier difficulties, UCLA collaborative group demonstrated that its SHSs were capable of achieving drag reduction, up to 70%, in a turbulent boundary layer (private communication). This group found visually that air pockets on its SHSs remained entrapped in water-tunnel experiments. This experimental observation motivated us to carry out the present numerical study, with the assumption that the air-water interface on SHSs would survive in turbulent flows.

III. NUMERICAL DETAILS

Direct numerical simulations of fully developed laminar and turbulent channel flows over SHSs were carried out using the same code by Min and Kim[23] except for a modification to accommodate a new boundary condition (see below). It was based on a semi-implicit, modified fractional step method, using second-order central difference method for all spatial derivatives. The computational domain of $6\delta \times 2\delta \times 3\delta$ was used in the streamwise, wall-normal, and spanwise directions, respectively. Table I shows the numerical grids used for different cases investigated in the present study.

We considered the same SHSs used by the UCLA group, where SHSs consisted of an array of microgrates oriented parallel to the flow direction. SHS was modeled through boundary conditions

TABLE I. Computational grids for turbulent channel flows.

Reynolds number		Number of grid points			Grid spacing		
Re_{τ_o}	Re_c	N_x	N_y	N_z	Δx^+	Δy^+_{min}	Δz^+
180	4200	128	129	128	8.4375	0.2911	4.2188
395	10 500	256	257	256	9.2578	0.3140	4.6289
590	16 700	384	257	384	9.2188	0.4689	4.6094

at the wall with alternating regions of no-slip (on the solid surface) and shear-free (on the air-water interface) boundary conditions between the microgrates [Fig. 3]. The interface was assumed to be flat, neglecting the deflection of the air-water interface.[25,27,28] A second-order implicit method was used for the shear-free boundary condition, in contrast to some earlier studies,[25,27] where a first-order method was used, as it was found that the latter led to non-negligible errors. Unless stated otherwise, SHS was applied to both walls of the channel in order to avoid possible influences from the other wall.

Two sets of parametric studies were performed by varying the pitch (P) and gas fraction (GF) of microgrates [Fig. 3]. Here GF is defined as $GF = (P - W)/P$, where W is the width of the microgrates. The first set was designed to fix $P/\delta = 0.375$ and varied GF as 0.5, 0.75, 0.875, 0.9375. The second was to fix $GF = 0.5$ and varied $P/\delta = 0.093\,75$, 0.1875, 0.375, 0.75, 1.5, and 3. In order to investigate the effect of Reynolds number on the performance of SHSs, computations were carried out at different Reynolds numbers of $Re_c = 100$, 1000, 1500, 2200, and 3000, for laminar flows. For turbulent flows, three Reynolds numbers were considered, $Re_c = 4200$, 10 500, and 16 700, corresponding to $Re_{\tau o} = 180$, 395, and 590, based on the wall-shear velocity on a regular channel wall ($u_{\tau o}$).

Periodic boundary conditions were used in the streamwise and spanwise directions. Unless stated otherwise, a constant mass flow rate was maintained, and skin-friction drag was computed from the required mean pressure gradient. The code was validated by comparing the present results with those of Min and Kim[23] and Martell *et al.*[27] An example of such validation is shown in Fig. 4.

IV. RESULTS AND DISCUSSIONS

A. The effective slip length

The effective slip length is very useful in understanding the effects of SHSs on skin-friction drag. It can be interpreted as a measure of influence into which SHS can affect the flow in the
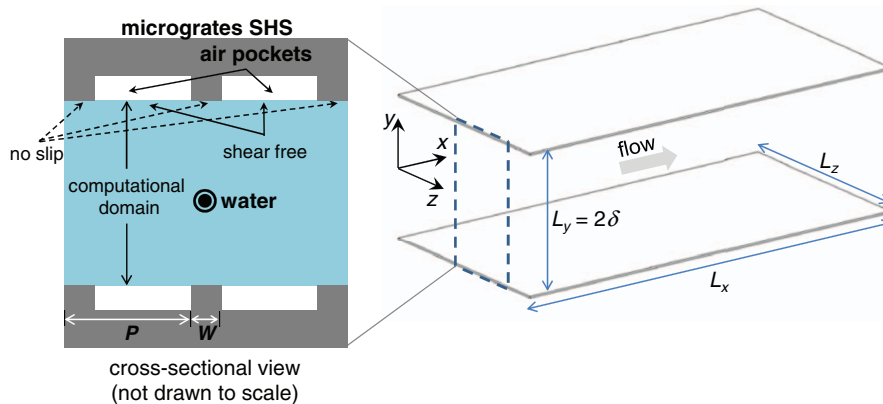

FIG. 3. Schematic illustration of the computational domain for turbulent channel flows. The upper and lower walls consist of repeating no-slip and slip boundary conditions to model the microgrates oriented parallel to the flow direction on SHS. The geometric parameters of microgrates on the current SHS are also defined.
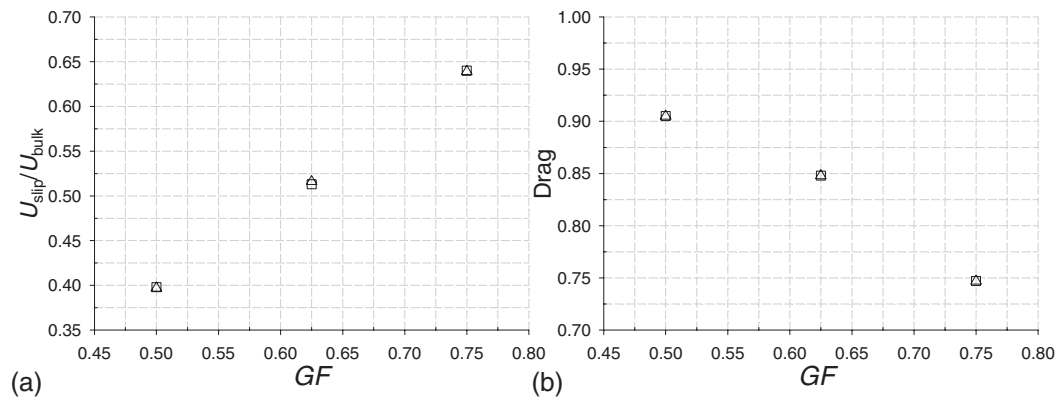
FIG. 4. Validation of the present numerical simulation compared with the results by Martell et al.:[27] (a) slip velocity, U_{slip} (normalized to the bulk velocity, U_{bulk}); (b) normalized drag. Note that the SHS was applied on the lower wall only. △, Martell et al.;[27] □, present results.

wall-normal direction. The effective slip length was calculated from the computed mean velocity profiles averaged over the micrograties, and then by applying the definition of the slip length shown in Fig. 1(b). Figure 5 shows the effective slip length as a function of GF in fully developed laminar and turbulent channel flows. For laminar channel or pipe flows with structured (e.g., micrograties and microposts) SHSs, a theoretical relationship between the effective slip length and the surface geometry has been proposed[34, 35] and confirmed experimentally[3] and numerically.[11, 18, 36] The present results are also in good agreement with the theoretical prediction. For turbulent flows, however, the effective slip length deviates from the theoretical prediction, and it decreases as Reynolds number increases. Note that at the smallest Reynolds number considered for the present study ($Re_{\tau o} = 180$), the effective slip length closely follows the theoretical prediction. This is consistent with other results since at this low Re_τ, most near-wall turbulence structures were suppressed by SHS and the flow, at the near-wall region in particular, was almost laminarized. The effective slip length in turbulent flows not only depends on the geometry of SHS, but also depends on details of flow conditions on SHS, although the general trend remains the same (i.e., it increases with GF).
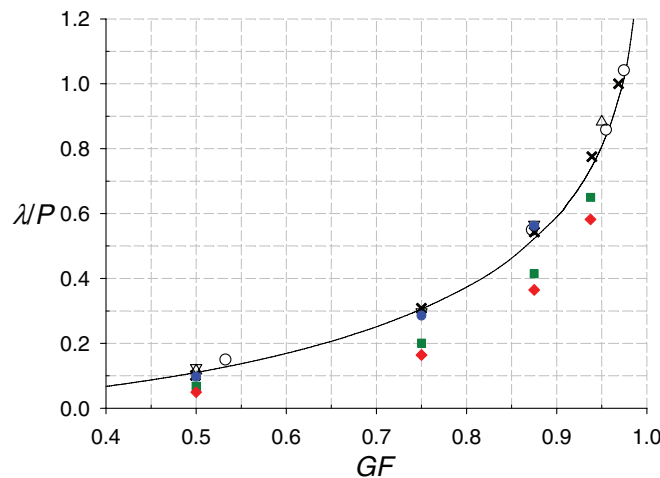

FIG. 5. Variations of normalized effective slip length (λ/P) with GF of longitudinal micrograties on SHS in channel flows, where P denotes the pitch of the micrograties ($P/\delta = 0.375$): — , theoretical prediction for laminar flow;[34] ○, Lee et al.[3] (laminar, experiment); ×, Maynes et al.;[11] △, Cheng et al.;[36] ▼, present (laminar, simulation); ● (blue), present (turbulent, $Re_{\tau o} = 180$); ■ (green), present (turbulent, $Re_{\tau o} = 395$); ♦ (red), present (turbulent, $Re_{\tau o} = 590$) (simulation).

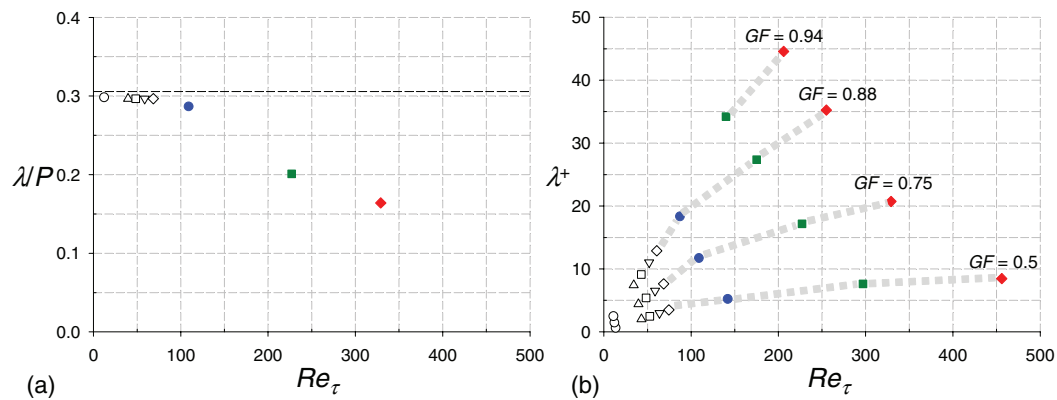FIG. 6. Variations of effective slip length (a) normalized to the pitch (λ/P) and (b) in wall units (λ^+) with Re_τ on SHSs in fully developed channel flows ($P/\delta = 0.375$): $\circ$, $Re_c = 100$; $\triangle$, $Re_c = 1000$; $\square$, $Re_c = 1500$; $\triangledown$, $Re_c = 2200$; $\diamond$, $Re_c = 3000$ (laminar flows); $\bullet$ (blue), $Re_{\tau o} = 180$; $\blacksquare$ (green), $Re_{\tau o} = 395$; $\blacklozenge$ (red), $Re_{\tau o} = 590$ (turbulent flows). In (a), dashed line denotes the theoretical prediction for a laminar channel flow with SHSs[34] and the GF is fixed at 0.75.

Figure 6(a) shows an example of the dependence of the effective slip length on Re_τ for a given SHS geometry ($P/\delta = 0.375$ and $GF = 0.75$). Note that Re_τ is based on the wall-shear velocity on SHS, and so it is lower than $Re_{\tau o}$, which is based on the wall-shear velocity in a regular channel under the same condition. It also shows that the effective slip length is independent of Re_τ in laminar flows, but decreases as Re_τ increases in turbulent flows. The same trends were observed (not shown here) with different GFs. It is important to point out that although the physical value of the effective slip length for a given SHS decreases as Reynolds number increases, the effective slip length normalized by viscous wall units, $\lambda^+ = \lambda u_\tau/\nu$, increases as Reynolds number increases as shown in Fig. 6(b). This is significant for high Reynolds number applications, since it is λ^+ that determines how much skin-friction drag reduction can be achieved (see Sec. IV B). This is also good news for real engineering applications, where maintaining stable air-water interfaces becomes difficult in harsh environments, and the pitch of SHSs must be kept small for stability of the interface. In high Reynolds number flows, a relatively small pitch must be used for the purpose of more robust air-water interfaces, but the relevant non-dimensional effective slip length can be large enough to have an impact on skin-friction drag in turbulent flows.

B. Skin-friction drag

Figure 7 shows the variation of skin-friction drag on SHSs with Re_τ and GF. Recall that the skin-friction drag was calculated from the mean pressure gradient required to maintain the same flow rate as that in a regular channel, and that the skin-friction drag on SHSs was normalized by that of the regular channel flow. The pitch of the micrograts is fixed at $P/\delta = 0.375$. In the laminar flow regime, the drag reduction is independent of Reynolds number [Fig. 7(a)], but it increases with GF [Fig. 7(b)]. Since the drag reduction in laminar flows is a direct consequence of the effective slip, its variation with Re_τ and GF shows the same behavior as the variation of the effective slip length shown in Fig. 6. For a given SHS (i.e., the same GF), the drag reduction in turbulent flows is much larger than that in laminar flows, and it increases with Reynolds number, implying an additional mechanism by which the drag reduction is achieved in turbulent flows. Note that although the initial Reynolds numbers ($Re_{\tau o}$) on regular channel walls is the same (180, 395, and 590), the resulting Re_τ on SHSs becomes smaller as GF increases [Fig. 7(a)]. In Fig. 7(b), the effect of GF is shown more clearly. The effect of Reynolds number becomes less pronounced at high GF (>0.9). This implies that once the non-dimensional effective slip length reaches a certain value, a further increase no longer affects skin-friction drag (see below for further discussion on this point).

The effect of the pitch of the micrograts on the effective surface slip length and skin-friction drag is shown in Fig. 8. Here, we varied the pitch of the micrograts (i.e., the number of micrograts
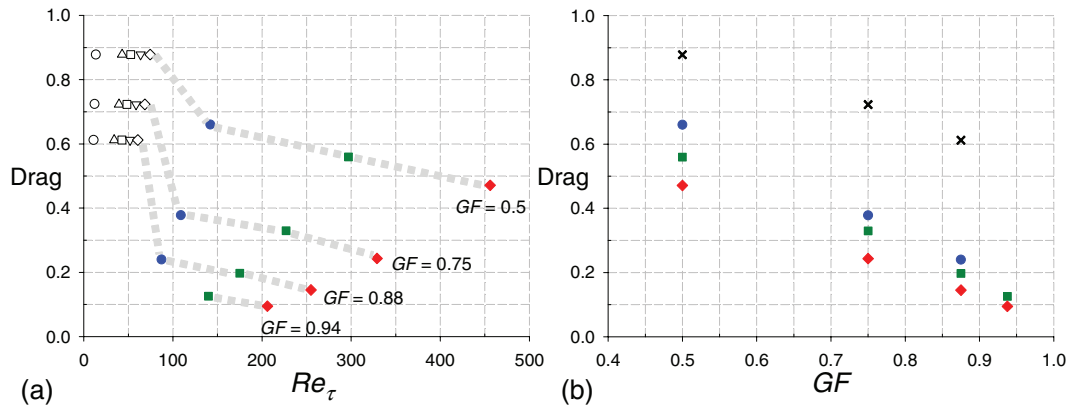
FIG. 7. Variations of the normalized drag with (a) Re_τ and (b) GF in fully developed channel flows ($P/\delta = 0.375$): $\circ$, $Re_c = 100$; $\triangle$, $Re_c = 1000$; $\square$, $Re_c = 1500$; $\triangledown$, $Re_c = 2200$; $\diamond$, $Re_c = 3000$ (laminar flows); $\bullet$ (blue), $Re_{\tau o} = 180$; $\blacksquare$ (green), $Re_{\tau o} = 395$; $\blacklozenge$ (red), $Re_{\tau o} = 590$ (turbulent flows). Here, the pitch of the micrograles is fixed at $P/\delta = 0.375$. In (b), "$\times$" denotes the data in laminar flows (independent of Reynolds number).

in a fixed computational domain) as $P/\delta = 0.1875, 0.375, 0.75, 1.5$, and 3 with fixed $GF = 0.5$. Note that the actual reduced wall-shear velocity (u_τ) on each SHS was used to non-dimensionalize the flow variables. Figure 8(a) shows how the effective slip length (λ^+) varies with the pitch (P^+): λ^+ increases sharply and then gradually saturates when $P^+ > 200$. Variations of the normalized drag with P^+ in Fig. 8(b) show the same trend: that is, a sharp decrease up to $P^+ \sim 200$, followed by no change afterward. The maximum possible drag reduction with $GF = 0.5$ is approximately 50% (due to the edge effect between micrograles and shear-free zones), which was attained when $P^+ > 200$. Note that for $GF = 0.5$ and $P^+ = 200$, the width of the air-water interface (i.e., the shear-free zone) is 100 in viscous wall units, which corresponds to the mean spacing of near-wall streaky structures. It appears that the relative size between the pitch of micrograles and near-wall turbulence structures, both in terms of viscous wall units, is an important factor in determining skin-friction drag on SHSs.

The data shown in Fig. 8 are from three different Reynolds numbers for a fixed gas fraction ($GF = 0.5$), thus demonstrating the relevance of viscous wall units in consideration of the effects of SHSs on skin-friction drag. Motivated by the collapse of λ^+ from different Reynolds numbers, we examined the skin-friction drag for all cases (i.e., different Re, GF, P) as a function of λ^+ as shown in Fig. 9. The data collapse remarkably well, thus demonstrating the relevance of λ^+ in determining skin-friction drag on SHSs. The normalized drag decreases rapidly as λ^+ increases up to about
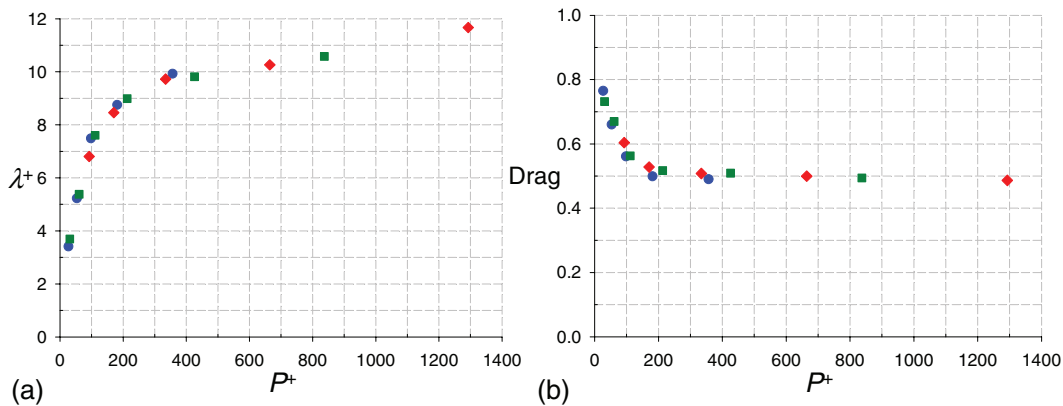

FIG. 8. Variations of (a) the effective slip length (λ^+) and (b) normalized drag with the pitch of micrograles (P^+) in fully developed turbulent channel flows ($GF = 0.5$): $\bullet$ (blue), $Re_{\tau o} = 180$; $\blacksquare$ (green), $Re_{\tau o} = 395$; $\blacklozenge$ (red), $Re_{\tau o} = 590$. Note that all variables were normalized with the wall-shear velocity (u_τ) on SHSs.
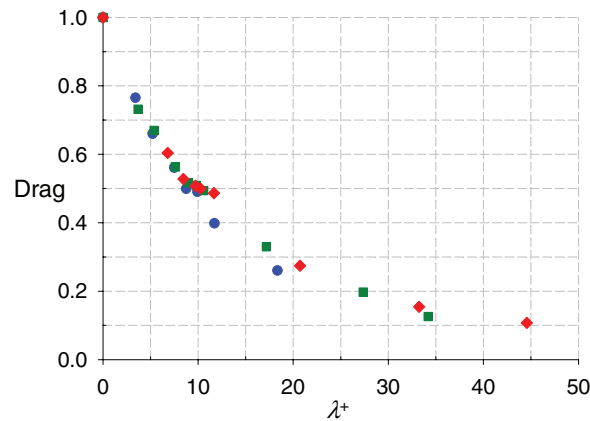
FIG. 9. Variation of normalized drag with the effective slip length in wall units (λ^+) in fully developed turbulent channel flows: ● (blue), $Re_{\tau o} = 180$; ■ (green), $Re_{\tau o} = 395$; ♦ (red), $Re_{\tau o} = 590$.

30–40, followed by little change. This is consistent with the earlier observation that skin-friction drag became independent of Reynolds number at high *GF* [Fig. 7(b)], since for a given geometry of SHS, λ^+ increases as Reynolds number increases, but once it reaches about $\lambda^+ \simeq$ 30–40, it does not affect the drag any further. Note that this condition of saturation would occur at a lower Reynolds number for SHS with a higher GF, which has a larger λ and hence attains $\lambda^+ \simeq$ 30–40 at a lower Reynolds number. This is indeed the case as shown in Fig. 7(b). Since the effective slip length can be interpreted as a depth of influence into which SHSs affect the flow in the wall-normal direction, the results shown in Fig. 9 imply that for maximum drag reduction, the depth of influence must include the buffer layer of wall-bounded turbulent flows.

C. Turbulence structures

The fact that skin-friction drag reduction in turbulent flows is larger than that in laminar flows for the same SHS implies that there must be an additional effect aside from the effective slip, by which the drag reduction in laminar flows is achieved. It has been generally accepted that near-wall turbulence structures, streamwise vortices in particular, play a critical role in producing high skin-friction drag in wall-bounded turbulent flows. Many control strategies have been designed to control near-wall streamwise vortices (see, for example, Kim[37]). However, there have been contradictory results as to how SHSs affect near-wall turbulence structures. Min and Kim[23] reported that a hydrophobic surface with streamwise slip led to weakened near-wall turbulence structures, which in turn resulted in reduced skin-friction drag. Martell *et al.*,[25] on the other hand, reported that SHSs did not affect the nature of near-wall turbulence structures but simply shifted them toward SHSs. Since Min and Kim[23] modeled their hydrophobic surface with a specified slip length, while Martell *et al.*[25] modeled with a shear-free boundary condition (the same as used for the present study), we repeated some calculations of Martell *et al.*[25] using the shear-free boundary condition to see if the difference was due to the boundary condition used in each study. Figure 10 shows an example of these calculations, in which only one side of the channel walls (lower wall in this example) was SHS. Also for this calculation, we used a fixed mean pressure gradient as was done by Martel *et al.*[25,27] It is apparent from Fig. 10 that SHS at the lower wall weakened near-wall vortical structures, in agreement with the conclusion drawn by Min and Kim.[23] This result is also consistent with the notion that it is the near-wall shear that generates and maintains near-wall streamwise vortices. In the absence of the shear on the air-water interfaces of SHSs, these vortices cannot be sustained, resulting in a lower skin-friction drag on SHSs.

Figure 11 further demonstrates the effect of SHS on turbulence structures. All calculations were started from a regular channel flow at $Re_{\tau o} = 590$ for $P/\delta = 0.375$. SHSs with three different *GF* were used for comparison. Note that both walls were SHSs. As *GF* increases (so does the effective
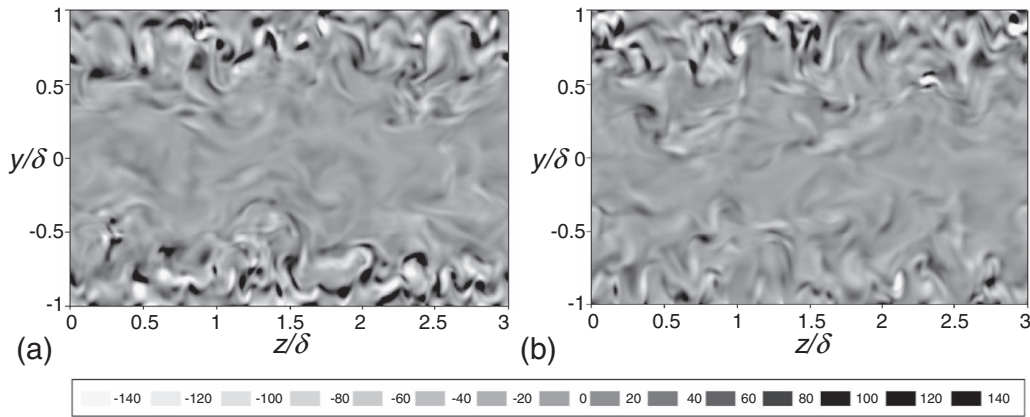
FIG. 10. Contours of streamwise vorticity in $y–z$ plane for $P/\delta = 0.375$: (a) regular channel ($Re_{\tau_o} = 395$); (b) $GF = 0.5$ ($Re_\tau = 395$). SHS is applied only at the lower wall. Grey-scale levels are from -140 to 140 in increments of 20.

slip length), near-wall vortical structures disappear, resulting in smaller skin-friction drag. This demonstrates that there is a strong correlation between the strength of near-wall streamwise vortices and skin-friction drag. The streamwise vortices primarily reside within the buffer layer, and the earlier observation that skin-friction drag does not decrease any further after λ^+ reaches about 40 can be understood in the same context.

The effects of slip in different directions have also been explained in relation to the modification of near-wall turbulence structures.[23,24] For example, it was found that spanwise slip led to stronger
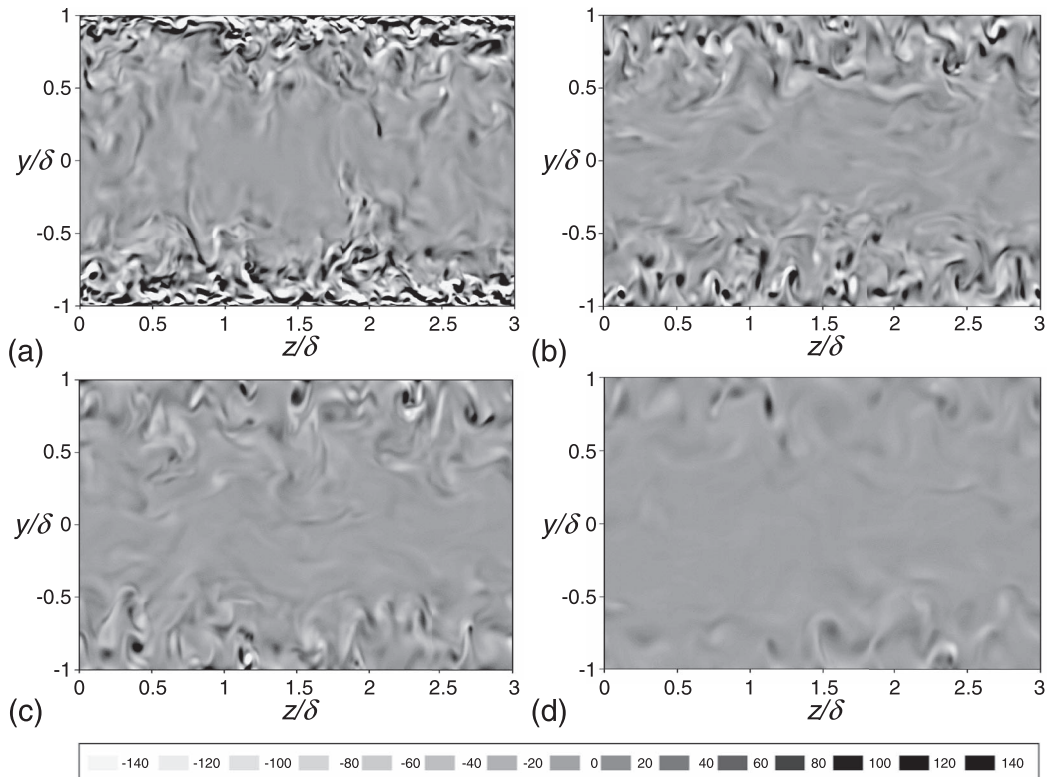

FIG. 11. Contours of streamwise vorticity in $y–z$ plane for $P/\delta = 0.375$: (a) regular channel ($Re_{\tau_o} = 590$, $\lambda^+ = 0$); (b) $GF = 0.5$ ($Re_\tau = 456$, $\lambda^+ = 8.46$); (c) $GF = 0.75$ ($Re_\tau = 329$, $\lambda^+ = 20.7$); (d) $GF = 0.9375$ ($Re_\tau = 206$, $\lambda^+ = 44.57$). Grey-scale levels are from -140 to 140 in increments of 20.

streamwise vortices, resulting in increased skin-friction drag.[23] It is worth noting that in our present model of SHSs, we considered streamwise slip only, but actual SHSs will have both streamwise and spanwise slips, the characteristic of which would depend on SHS geometries (e.g., microgrates aligned in the streamwise direction induce a larger streamwise slip). Thus, the effects of actual SHSs are expected to be less than the present numerical results, which assumed no slip in the spanwise direction.

V. SUMMARY AND CONCLUDING REMARKS

Encouraged by the recent experimental observation that an SHS, consisting of microgrates aligned in the flow direction, could remain superhydrophobic (i.e., air pockets entrapped within microgrates), resulting in significant skin-friction drag reduction in a turbulent boundary layer, we conducted direct numerical simulations of turbulent channel flows in order to gain further insight into the effects of the same SHS on skin-friction drag. SHS was modeled through a shear-free boundary condition, assuming that the air-water interfaces were flat. It was found that drag-reduction in turbulent flows was much larger than that of laminar flows with the same SHS. Examinations of turbulence structures revealed that near-wall streamwise vortices on SHS were significantly modified, resulting in significantly reduced skin-friction drag. The amount of drag reduction in turbulent flows depended on SHS geometries and Reynolds number in contrast to laminar flows, where it depended solely on SHS geometries. Examinations of the effect of SHS geometries (i.e., the pitch and *GF*) revealed that once the width of the air-water region (i.e., shear-free region) became on the order of the width of near-wall streaky structures, a minimum drag state was reached. It was also shown that the amount of drag reduction for different SHSs and Reynolds numbers was well correlated with the effective slip length normalized by viscous wall units. In addition, skin-friction drag decreased as the effective slip length increased, but the effect diminished after the effective slip length reached about 40 viscous wall units, indicating that turbulence structures within the buffer region were primarily responsible for high skin-friction in wall-bounded turbulent shear flows.

Most existing numerical simulations, including the present study, have been performed with the assumption that the air-water interface is flat. Some investigators[38,39] have examined the effect of air-water interface curvature on the effective slip length on SHSs similar to the present study. They found that the effective slip length in laminar channel flows changed significantly depending on the deformation or protrusion of the air-water interface and the ratio of the pitch to the channel height. The effects of the actual morphology of the air-water interface on the effective slip length and other relevant characteristics of SHSs need to be addressed in the future.

Finally, we assumed in this study that the air-water interface would not break down in turbulent flows. There has been some evidence that it would be more difficult to keep air entrapped inside the microgrates in high Reynolds number turbulent flows, which, we believe, partially explains some inconsistent experimental results. The exact cause and mechanism by which the interface breaks down should also be addressed in a future study.

ACKNOWLEDGMENTS

[1] C.-H. Choi and C.-J. Kim, "Large slip of aqueous liquid flow over a nano-engineered superhydrophobic surface," Phys. Rev. Lett. **96**, 66001 (2006).

[2] J. P. Rothstein, "Slip on superhydrophobic surfaces," Annu. Rev. Fluid Mech. **42**, 89 (2010).

[3] C. Lee, C.-H. Choi, and C.-J. Kim, "Structured surfaces for a giant liquid slip," Phys. Rev. Lett. **101**, 064501 (2008).

[4] C. Lee and C.-J. Kim, "Maximizing the giant liquid slip on superhydrophobic microstructures by nanostructuring their sidewalls," Langmuir **25**, 12812 (2009).

[5] R. Fürstner, W. Barthlott, C. Neinhuis, and P. Walzel, "Wetting and self-cleaning properties of artificial superhydrophobic surfaces," Langmuir **21**, 956 (2005).

[6] G. Fang, W. Li, X. Wang, and G. Qiao, "Droplet motion on designed microtextured superhydrophobic surfaces with tunable wettability," Langmuir **24**, 11651 (2008).

[7] J. Genzer and K. Efimenko, "Recent developments in superhydrophobic surfaces and their relevance to marine fouling: a review," Biofouling **22**, 339 (2006).

[8] S. Jung, M. Dorrestijn, D. Raps, A. Das, C. M. Megaridis, and D. Poulikakos, "Are superhydrophobic surfaces best for icephobicity?," Langmuir **27**, 3059 (2011).

[9] M. A. Samaha, H. V. Tafreshi, and M. Gad-el Hak, "Influence of flow on longevity of superhydrophobic coatings," Langmuir **28**, 9759 (2012).

[10] C. Lee and C.-J. Kim, "Underwater restoration and retention of gases on superhydrophobic surfaces for drag reduction," Phys. Rev. Lett. **106**, 14502 (2011).

[11] D. Maynes, K. Jeffs, W. Woolford, and B. W. Webb, "Laminar flow in a microchannel with hydrophobic surface patterned microribs oriented parallel to the flow direction," Phys. Fluids **19**, 093603 (2007).

[12] J. Ou and J. P. Rothstein, "Direct velocity measurements of the flow past drag-reducing ultrahydrophobic surfaces," Phys. Fluids **17**, 103606 (2005).

[13] B. Bhushan and Y. C. Jung, "Natural and biomimetic artificial surfaces for superhydrophobicity, self-cleaning, low adhesion, and drag reduction," Prog. Mater. Sci. **56**, 1 (2011).

[14] G. McHale, M. I. Newton, and N. J. Shirtcliffe, "Immersed superhydrophobic surfaces: gas exchange, slip and drag reduction properties," Soft Matter **6**, 714 (2010).

[15] L. Bocquet and E. Lauga, "A smooth future?," Nature Mater. **10**, 334 (2011).

[16] A. M. J. Davis and E. Lauga, "Hydrodynamic friction of fakir-like superhydrophobic surfaces," J. Fluid Mech. **661**, 402 (2010).

[17] J. Davies, D. Maynes, B. W. Webb, and B. Woolford, "Laminar flow in a microchannel with superhydrophobic walls exhibiting transverse ribs," Phys. Fluids **18**, 087110 (2006).

[18] W. Woolford, D. Maynes, and B. W. Webb, "Liquid flow through microchannels with grooved walls under wetting and superhydrophobic conditions," Microfluid Nanofluid **7**, 121 (2009).

[19] K. Watanabe, H. Yanuar, and H. Udagawa, "Drag reduction of Newtonian fluid in a circular pipe with a highly water-repellent wall," J. Fluid Mech. **381**, 225 (1999).

[20] J. Ou, B. Perot, and J. P. Rothstein, "Laminar drag reduction in microchannels using ultrahydrophobic surfaces," Phys. Fluids **16**, 4635 (2004).

[21] R. Truesdell, A. Mammoli, P. Vorobieff, F. Swol, and J. C. Brinker, "Drag reduction on a patterned superhydrophobic surface," Phys. Rev. Lett. **97**, 44504 (2006).

[22] Y. C. Jung and B. Bhushan, "Biomimetic structures for fluid drag reduction in laminar and turbulent flows," J. Phys.: Condens. Matter **22**, 035104 (2010).

[23] T. Min and J. Kim, "Effects of hydrophobic surface on skin-friction drag," Phys. Fluids **16**, L55 (2004).

[24] A. Busse and N. D. Sandham, "Influence of an anisotropic slip-length boundary condition on turbulent channel flow," Phys. Fluids **24**, 055111 (2012).

[25] M. B. Martell, J. P. Rhothstein, and B. Perot, "An analysis of superhydrophobic turbulent drag reduction mechanisms using direct numerical simulation," Phys. Fluids **22**, 065102 (2010).

[26] K. Fukagata, N. Kasagi, and P. Koumoutsakos, "A theoretical prediction of friction drag in turbulent flow by superhydrophobic surfaces," Phys. Fluids **18**, 051703 (2006).

[27] M. B. Martell, B. Perot, and J. P. Rhothstein, "Direct numerical simulations of turbulent flows over superhydrophobic surfaces," J. Fluid Mech. **620**, 31 (2009).

[28] K. Jeffs, D. Maynes, and B. W. Webb, "Prediction of turbulent channel flow with superhydrophobic walls consisting of micro-ribs and cavities oriented parallel to the flow direction," Int. J. Heat Mass Transfer **53**, 786 (2010).

[29] C. Henoch, T. N. Krupenkin, P. Kolodner, M. S. Taylor, J. A. Hodes, A. M. Lyons, C. Peguero, and K. Breuer, "Turbulent drag reduction using superhydrophobic surfaces," AIAA Paper 2006-3192, 2006.

[30] R. J. Daniello, N. E. Waterhouse, and J. P. Rothstein, "Drag reduction in turbulent flows over superhydrophobic surfaces," Phys. Fluids **21**, 085103 (2009).

[31] B. Woolford, J. Prince, D. Maynes, and B. W. Webb, "Particle image velocimetry characterization of turbulent channel flow with rib patterned superhydrophobic walls," Phys. Fluids **21**, 085106 (2009).

[32] J. Zhao, X. Du, and X. Shi, "Experimental research on friction-reduction with superhydrophobic surfaces," J. Mar. Sci. Appl. **6**, 58 (2007).

[33] C. Peguero and K. Breuer, "On drag reduction in turbulent channel flow over superhydrophobic surface," in *Advances in Turbulence XII*, Springer Proceedings in Physics (Springer-Verlag, Berlin/Heidelberg, 2009).

[34] E. Lauga and H. A. Stone, "Effective slip in pressure-driven stokes flow," J. Fluid Mech. **489**, 55 (2003).

[35] C. Ybert, C. Barentin, and C. Cottin-Bizonne, "Achieving large slip with superhydrophobic surfaces: Scaling laws for generic geometries" Phys. Fluids **19**, 123601 (2007).

[36] Y. P. Cheng, C. J. Teo, and B. C. Khoo, "Microchannel flows with superhydrophobic surfaces: Effects of Reynolds number and pattern width to channel height ratio," Phys. Fluids **21**, 122004 (2009).

[37] J. Kim, "Control of turbulent boundary layer," Phys. Fluids **15**, 1093 (2003).

[38] M. Sbragaglia and A. Prosperetti, "A note on the effective slip properties for microchannel flows with ultrahydrophobic surfaces," Phys. Fluids **19**, 043603 (2007).

[39] C. J. Teo and B. C. Khoo, "Flow past superhydrophobic surfaces containing longitudinal grooves: effects of interface curvature," Microfluid. Nanofluid. **9**, 499 (2010).